RSC Advances

PAPER

Cite this: *RSC Adv.*, 2015, **5**, 45384

Adsorption behavior of Cr(VI) from aqueous solution onto magnetic graphene oxide functionalized with 1,2-diaminocyclohexanetetraacetic acid

Fang-ying Guo,[ab] Yun-guo Liu,*[ab] Hui Wang,[ab] Guang-ming Zeng,[ab] Xin-jiang Hu,[ab] Bo-hong Zheng,[c] Ting-ting Li,[ab] Xiao-fei Tan,[ab] Shu-fan Wang[ab] and Ming-ming Zhang[ab]

Received 2nd February 2015
Accepted 12th May 2015

DOI: 10.1039/c5ra02015h

www.rsc.org/advances

A novel magnetic composite adsorbent was synthesized by grafting 1,2-diaminocyclohexanetetraacetic acid to magnetic graphene oxide (DCTA/E/MGO). The DCTA/E/MGO was employed for removing Cr(VI) from aqueous solution in this study. The composite was characterized by FESEM, TEM, BET, XRD, FT-IR and XPS. The adsorption behaviors of Cr(VI) by DCTA/E/MGO in aqueous solution were systematically investigated. Second order kinetic and Freundlich isotherm models validated the experimental data. The adsorption rate was influenced by both film diffusion and intraparticle diffusion. Thermodynamic parameters revealed that the adsorption reaction was an endothermic and spontaneous process. The novel adsorbent exhibited better Cr(VI) removal efficiency in solutions with low pH. The decontamination of Cr(VI) by DCTA/E/MGO was influenced by ionic strength. These results are important for estimating and optimizing the removal of metal ions by the DCTA/E/MGO composite.

1. Introduction

Chromium is usually found in two common oxidation states, Cr(VI) and Cr(III). Usually Cr(VI) compounds are more toxic than Cr(III) because of their marked carcinogenic, teratogenic and mutagenic effects to humans and other living organisms.[1] Thus, it is necessary to remove Cr(VI) contaminants from wastewater before being released into the environment. Various methods of chromium removal have been well documented, including ion exchange, evaporation, chemical precipitation, membrane separation, adsorption, *etc.*[2] Among all of these methods, adsorption is one of the most economically favorable and technically easy methods.[3]

Normally, the adsorption ability of a material is controlled in part by the number of available functional groups. Graphene oxide (GO) prepared by Hummers method[4] contains a range of oxygen-containing functional groups on the surface, such as hydroxyl, epoxide, carbonyl and carboxyl groups.[5] These groups are available for removing heavy metals from wastewater. In addition, GO is characterized by a large specific surface area and can be readily obtained from cheap natural graphite in large scale.[6] From these points, GO is considered as a suitable adsorbent for the removal of pollutants in water. However, GO can be dispersed in aqueous media due to the oxygen-containing functional groups on its surface, therefore it is difficult to be separated from water after the adsorption process. The problem can be solved by loading magnetic nanoparticles to GO. The separation can be achieved by magnetic separation. The magnetic technology combines the advantages of adsorption with the merit of easy separation, but it has been found to have some negative effects on the adsorption capacity of the GO.[7,8]

In order to improve the adsorption ability and selectivity of GO for metal ions, a great number of GO derivates have been obtained by grafting new chemical substances on the GO backbone, such as sulfanilic acid,[4] EDTA,[5] chitosan[9] and ethylenediamine.[10] Meanwhile, 1,2-diaminocyclohexane-*N*,*N*,*N*′,*N*′-tetraacetic acid (DCTA), acting as a multidentate chelating ligand, can form strong complexes with most metals. These complexes have similar chemical structures to those formed with ethylenediaminetetraacetic acid (EDTA) but have higher stability constants for most metals.[11,12] Besides, among various functional groups, the amine group has a relatively high reactivity and can easily react with many chemicals.[2,8] Therefore, it is a feasible way to graft DCTA onto magnetic graphene oxide (MGO) through the ethylenediamine.

The main objectives of this work were to: (1) prepare DCTA/E/MGO composite and characterize it by FESEM, TEM, BET,

[a]*College of Environmental Science and Engineering, Hunan University, Changsha 410082, PR China. E-mail: nhxyhj111@163.com; Fax: +86 731 88822829; Tel: +86 731 88649208*

[b]*Key Laboratory of Environmental Biology and Pollution Control (Hunan University), Ministry of Education, Changsha 410082, PR China*

[c]*School of Architecture and Art, Central South University, Changsha 410082, PR China*

XRD, FT-IR and XPS; (2) study the adsorption mechanism with kinetics, isotherm and thermodynamic models; (3) evaluate the effects of process parameters on Cr(VI) removal, *i.e.*, pH, initial ion concentrations and temperature; (4) investigate the effects of ionic strength on Cr(VI) decontamination.

2. Materials and methods

2.1. Materials

Graphite powder was supplied by Tianjin Hengxin Chemical Preparation Co., Ltd., China. 1,2-Diaminocyclohexane-*N*,*N*,*N*′,*N*′-tetraacetic acid (DCTA) was purchased from Xiya Reagent Research Center (Shandong, China). Ethylenediamine was purchased from Shanghai Chemical Reagents Factory. The reagents 1-ethyl-3-(3-dimethylaminopropyl)carbodiimide hydrochloride (EDC), *N*-hydroxyl succinimide (NHS) were obtained from Shanghai Civi Chemical Technology Co., Ltd., China. All chemicals used in the experiments were analytical grade.

GO was synthesized *via* modified Hummers method[13] from the natural graphite powder. Briefly, graphite powders were first oxidized by concentrated H_2SO_4, $K_2S_2O_8$ and P_2O_5. Next, the concentrated H_2SO_4, $KMnO_4$ and $NaNO_3$ were used to oxidize the preoxidized graphite, then 30% H_2O_2 was added to eliminate the excess MnO_4^-, and the products were rinsed with HCl (10%) and Milli-Q water. The resulting solution was sonicated for 2 h. The magnetic graphene oxide (MGO) was prepared by coprecipitation method. Fe^{3+} and Fe^{2+} (molar ratio 2 : 1) were mixed in the GO solution with addition of ammonia solution to form Fe_3O_4–GO composite.[4,14]

The DCTA/E/MGO was prepared by reacting DCTA with MGO through ethylenediamine. 0.1 M EDC and 0.1 M NHS solution were added to the DCTA dispersion with continuous stirring for 2 h,[15,16] then ethylenediamine was added. The mixed system was

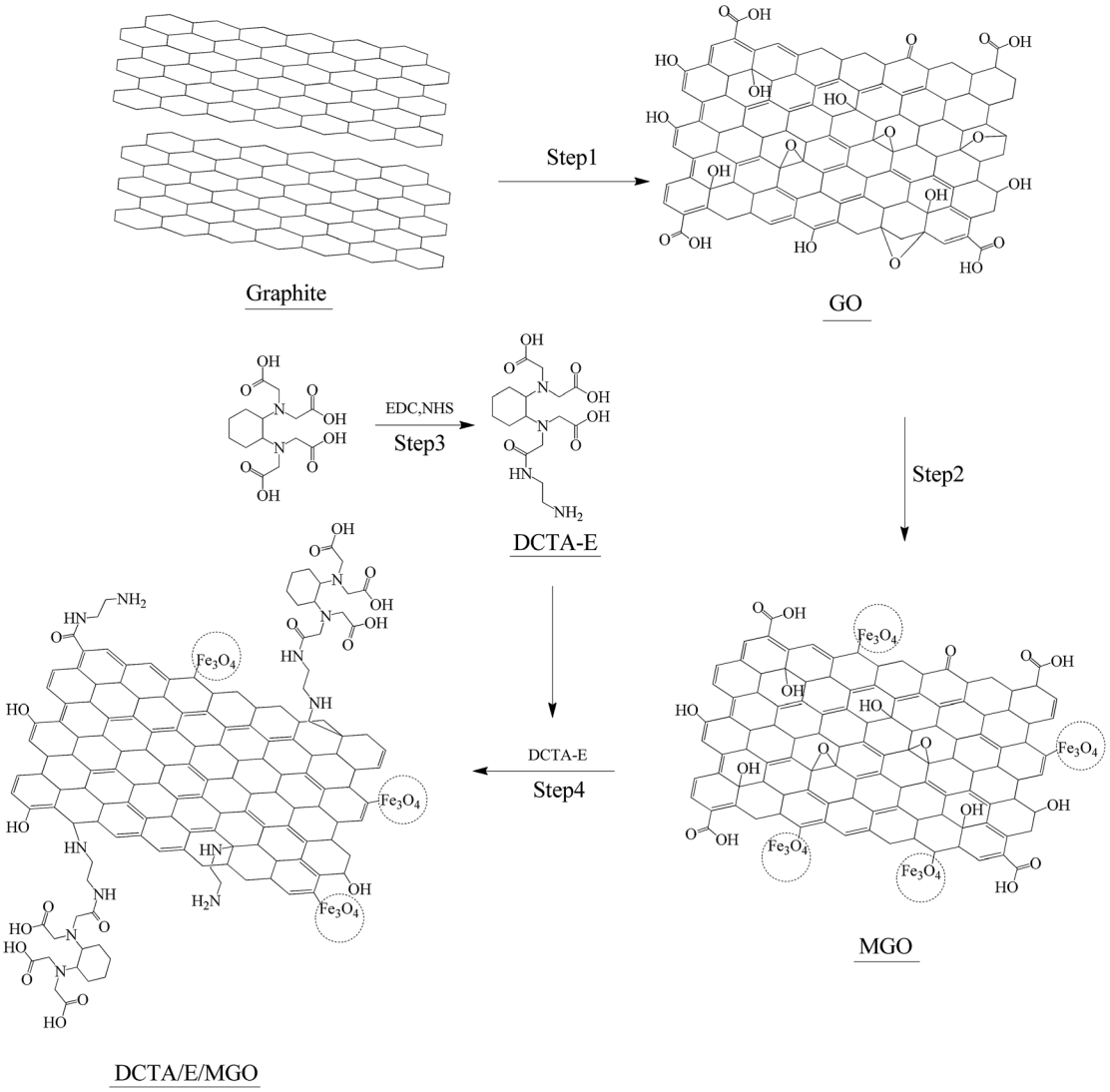

Fig. 1 The proposed scheme for the formation of DCTA/E/MGO: (Step 1) oxidation of natural graphite to graphite oxide, followed by ultrasonication; (Step 2) preparation of MGO by loading magnetic nanoparticles on the GO surface through chemical coprecipitation method; (Step 3) preparation of DCTA-E solution; (Step 4) formation of DCTA/E/MGO by grafting DCTA-E onto the MGO surface.

stirred continuously for 6 h in a water bath at 80 °C after being added into MGO dispersion.[8,15] The resulted product was washed repeatedly with Milli-Q water until pH was about neutral and finally stored at room temperature. The preparation sketch of DCTA/E/MGO is shown in Fig. 1.

2.2. Characterization

The morphology of the as-prepared adsorbent was characterized by field-emission scanning electron microscopy (FESEM, JSM 6700F, Japan) and transmission electron microscopy (TEM, Tecnai G2 F20, USA). The BET specific surface area was determined using nitrogen adsorption–desorption measurements (Autosorb-1, Quantachrome Instruments, USA). The X-ray diffraction (XRD) patterns of GO, MGO and DCTA/E/MGO composite were obtained on an X-ray diffractometer (Rigaku D/max-2500, Japan) with CuKα radiation. The FT-IR spectra of the DCTA/E/MGO and MGO were measured on a spectrophotometer (Varian 3100, USA) using the KBr pellet technique. The XPS measurements were performed using an ESCALAB 250Xi X-ray photoelectron spectrometer (Thermo Fisher, USA).

2.3. Adsorption experiments

A stock solution of Cr(VI) was prepared by dissolving 2.8287 g of 99.9% potassium dichromate ($K_2Cr_2O_7$) in 1000 mL of distilled water. The solutions of different Cr(VI) concentrations used in batch experiments were obtained by diluting the stock solution. All batch adsorption experiments were performed on an orbital shaker with a shaking speed of 150 rpm. For all the adsorption experiments, the suspension of MGO or DCTA/E/MGO was added to achieve the expected concentrations of the different components. Initial pH values of the Cr(VI) solutions were adjusted to the desired pH by adding negligible volumes of NaOH or HNO_3. After the adsorption process, the mixture was conveniently separated by a permanent magnet. The concentration of Cr(VI) in the supernatant was determined on a UV-vis spectrophotometer. The Cr(VI) removal at the equilibrium (q_e (mg g^{-1})) was calculated as follows:

$$q_e = \frac{(C_0 - C_e)V}{W} \quad (1)$$

where, C_0 and C_e (mg L^{-1}) are the initial and equilibrium concentrations of Cr(VI) ions, respectively; V is the volume of the solution (L); and W is the amount of adsorbent (g).

3. Results and discussion

3.1. Characterization of DCTA/E/MGO

The FESEM and TEM images of DCTA/E/MGO are demonstrated in Fig. 2. These images show that Fe_3O_4 particles are dispersed on the surface and some wrinkles are observed. The surface of the composite is rough, which can indicate an excellent possibility for the heavy metals to be trapped and adsorbed by the DCTA/E/MGO.

The N_2 adsorption–desorption isotherms (in Fig. 3a) were recorded to investigate the BET surface areas and pore structure of MGO and DCTA/E/MGO composite. The BET surface area of

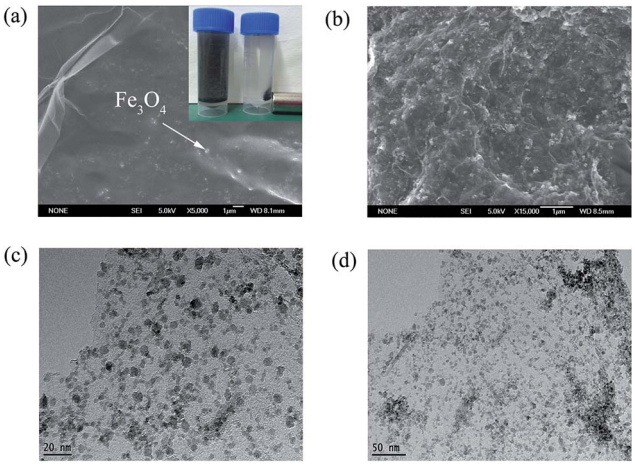

Fig. 2 (a) and (b) FESEM images of DCTA/E/MGO; (c) and (d) TEM images of DCTA/E/MGO.

the DCTA/E/MGO was measured to be 310.41 m^2 g^{-1}, which is much higher than that of MGO (114.61 m^2 g^{-1}). Nitrogen adsorption–desorption analysis shows all the DCTA/E/MGO and MGO samples with micro- and meso-porous structure. The pore size of DCTA/E/MGO samples mainly distribute at 1.4 nm (Fig. 3b). The introduction of DCTA led to a distinct increase in BET surface area which is beneficial for adsorption.

The XRD patterns of GO, MGO and DCTA/E/MGO are shown in Fig. 3c and d. For GO, a strong peak at $2\theta = 10.4°$ occurs, which is the structure expansion as oxygen-containing groups incorporate between the carbon sheets during the course of strong oxidation. For MGO and DCTA/E/MGO, the intense diffraction peaks at the Bragg angles of 30.09, 35.42, 37.05, 43.05, 53.39, 56.94 and 62.51 were observed clearly. These peaks are consistent with the (220), (311), (222), (400), (422), (511) and (440) facets of the cubic spinel crystal planes of Fe_3O_4 (JCPDS card no. 19-0629), respectively.[17] Compared with the pure GO diffracted signals, there are no diffracted signals for the GO sheets in MGO and DCTA/E/MGO, which is ascribed to that the strong signals of the iron oxides tend to overwhelm the weak carbon peaks.[18] Almost similar XRD patterns of MGO and DCTA/E/MGO were observed, which revealed that the synthesized process did not change the crystalline phase of Fe_3O_4. But, it was not sufficient to exclude the existence of γ-Fe_2O_3. However, the magnetic properties of γ-Fe_2O_3 are similar to Fe_3O_4, so there was no negative impact on the following experiments whether γ-Fe_2O_3 was contained in the samples or not.[19]

The FT-IR spectra of MGO and DCTA/E/MGO in the range of 4000–500 cm^{-1} are shown in Fig. 3e. The FTIR spectra of MGO and DCTA/E/MGO show the presence of O–H at 3449 cm^{-1}. In the FT-IR spectrum of MGO, the peak at 1730 cm^{-1} corresponding to C=O of carboxyl group on the GO shifts to 1643 cm^{-1} may be due to the formation of $-COO^-$ after coating with Fe_3O_4.[4] The stretching band of Fe–O peak appears at around 580 cm^{-1}. While in the FT-IR spectrum of DCTA/E/MGO, the bands at 1636 and 1616 cm^{-1} correspond to the characteristic C=O stretching vibration of –NHCO– (amide I)

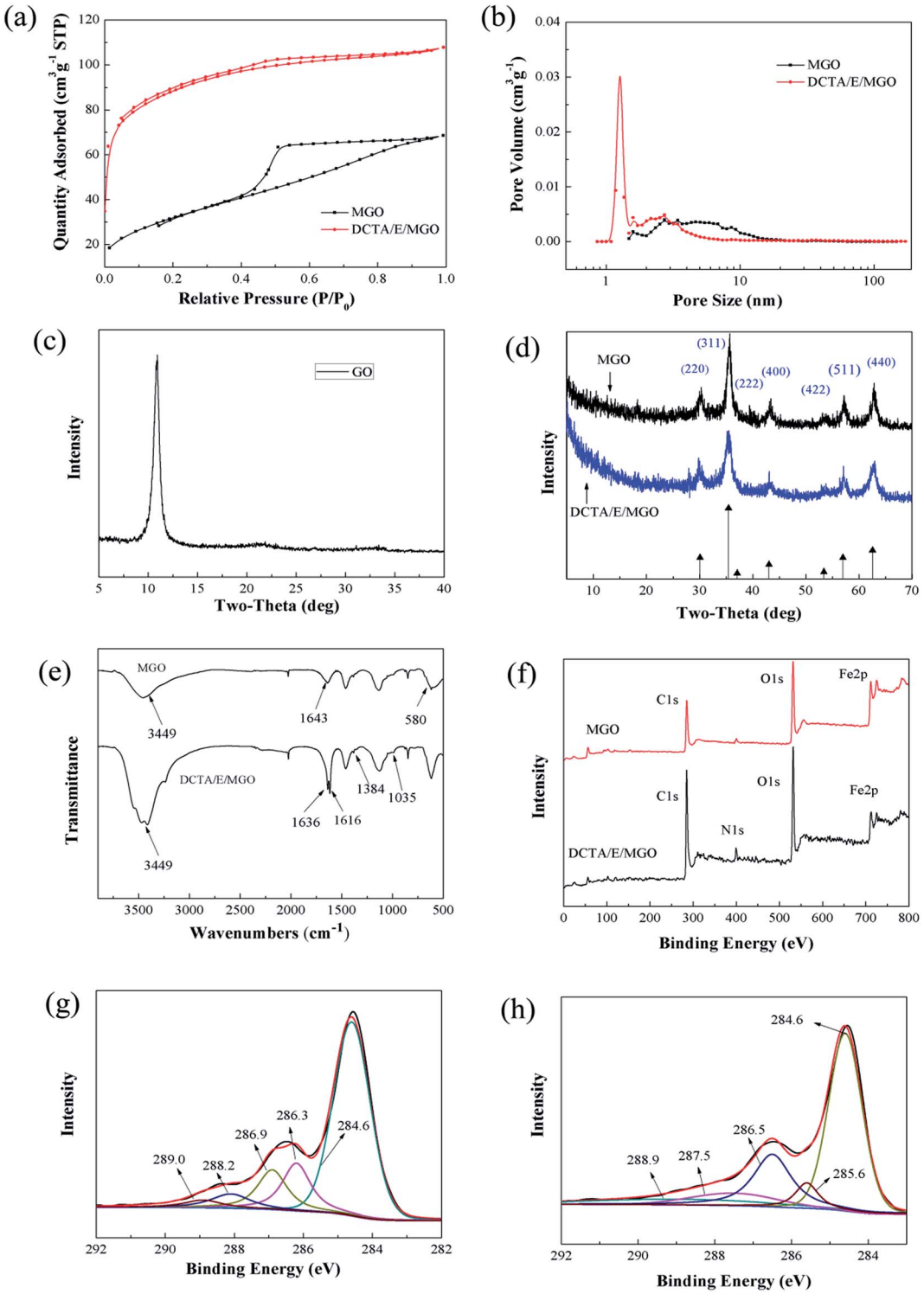

Fig. 3 Nitrogen adsorption–desorption isotherms (a) and pore size distribution (b) of MGO and DCTA/E/MGO; (c) and (d) XRD patterns of GO, MGO and DCTA/E/MGO; (e) FT-IR spectra of MGO and DCTA/E/MGO; (f) XPS wide-scan of MGO and DCTA/E/MGO; (g) and (h) C1s XPS spectra of MGO and DCTA/E/MGO.

and the N–H bending of $-NH_2$, respectively.[8,20] The peaks at 1035 and 1384 cm^{-1} correspond to C–O–C stretching vibration and C–OH stretching, respectively.[17] After the chemical grafting, the bands at 1636 and 1616 cm^{-1} appeared, demonstrating that DCTA and ethylenediamine were successfully grafted on MGO.

The chemical state of element in MGO and DCTA/E/MGO was further investigated by XPS. The wide scan XPS spectrum (Fig. 3f) of DCTA/E/MGO shows photoelectron lines at binding energies of about 285, 400, 530, and 711 eV which are attributed to C1s, N1s, O1s, and Fe2p, respectively.[21] The XPS survey of

DCTA/E/MGO indicates significant amount of N1s comparing to that of MGO (Fig. 3f), which is originated from the grafted ethylenediamine and DCTA. The elemental analysis illustrates a considerable increase in O/C atomic ratio in the DCTA/E/MGO (0.44) comparing to that of the MGO (0.31), which may be attributed to the high O/C atomic ratio of the introduced DCTA. In addition, five different peaks (Fig. 3g) centered at 284.6 eV, 286.3 eV, 286.9 eV, 288.2 eV and 289.0 eV are observed, corresponding to C–C, C–O, C–O–C, C=O and O–C=O groups of MGO, respectively.[22] The C1s spectrum of DCTA/E/MGO (Fig. 3h) can be curve-fitted into five peak components with binding energies of about 284.6, 285.6, 286.5, 287.5 and 288.9 eV, which attribute to the carbon atoms in the forms of C–C, C–N, C–O, HNC=O and O–C=O species, respectively.[8,23,24] Additional C–N and HNC=O species functions are observed. Thus, it can be concluded that DCTA has been grafted successfully to the MGO surface.

3.2. Adsorption kinetics

The adsorption kinetics is an important parameter for determination of the optimum adsorption time. The kinetic studies for Cr(VI) adsorption on the DCTA/E/MGO were carried out at three different Cr(VI) concentrations (10, 20, and 40 mg L^{-1}) and the results are given in Fig. 4a. It is shown that the amount of adsorbed Cr(VI) increased rapidly over the first 6 h of contact time. Furthermore, three kinetic models were tested to analyze the adsorption process, including pseudo-first-order kinetic model, pseudo-second-order kinetic model and intraparticle diffusion model. Fig. 4b and c show the pseudo-first-order and pseudo-second-order kinetics for the adsorption of Cr(VI) onto DCTA/E/MGO, respectively. These two kinetic models can be expressed as follows:[25]

$$\log(q_e - q_t) = \log(q_e) - \frac{k_1 t}{2.303} \quad (2)$$

$$\frac{t}{q_t} = \frac{1}{k_2 q_e^2} + \frac{t}{q_e} \quad (3)$$

where k_1 is the rate constant of pseudo-first-order adsorption (min^{-1}); k_2 is the rate constant of pseudo-second-order adsorption (g mg^{-1} min^{-1}); q_e and q_t are the amounts of Cr(VI) adsorbed at equilibrium and at any time t, respectively (mg g^{-1}).

The kinetic parameters calculated from the two models are listed in Table 1. From Table 1, it is noticed that the R^2 values of pseudo-second-order model (0.999, 0.998, and 0.998) are higher than those of pseudo-first-order model (0.894, 0.911, and 0.955). In addition, the calculated q_e values of the pseudo-second-order model agree with the experimental data better than those of the pseudo-first-order model. Based on these data, it can be concluded that the Cr(VI) uptake process complies with the second-order type kinetic reaction, which indicates that the rate-limiting step may be due to the chemical adsorption, high specific surface area and the absence of internal diffusion resistance.[8,26,27] It is also notable that the constant rate k_2 decreases with the increase of initial Cr(VI) concentration, which may be connected with the longer time required to reach the equilibrium state.[28]

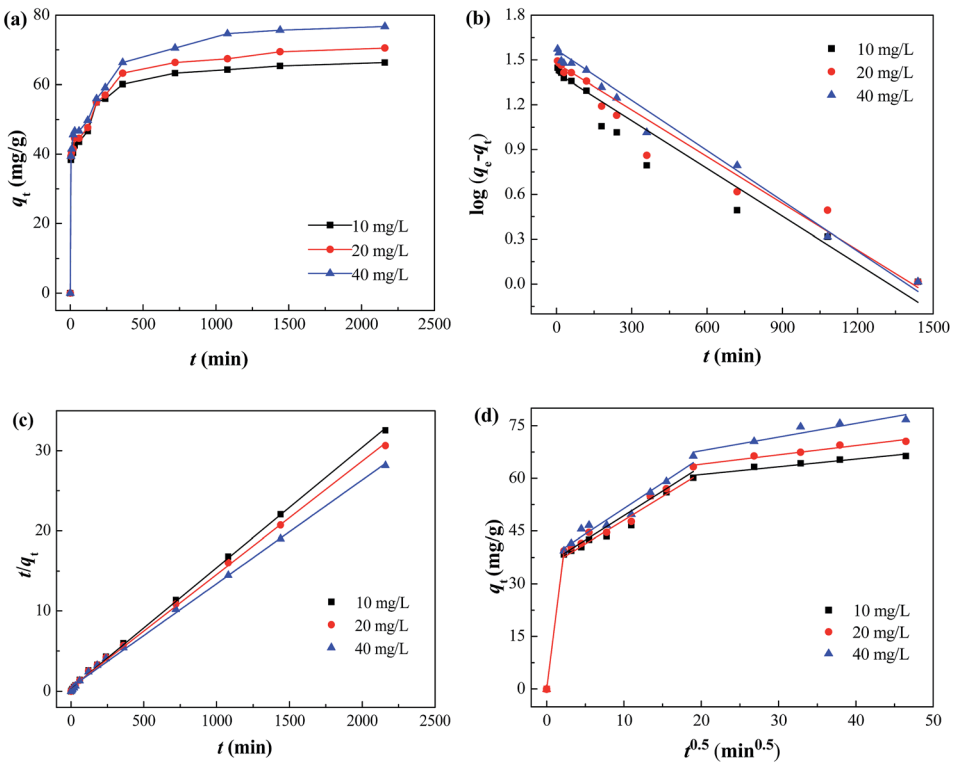

Fig. 4 (a) Time-dependent Cr(VI) sorption on DCTA/E/MGO at three different concentrations (10, 20 and 40 mg L^{-1}); (b) pseudo-first-order sorption kinetics; (c) pseudo-second-order sorption kinetics; (d) intraparticle diffusion kinetics (pH = 3.0 ± 0.1, T = 30 °C, t = 24 h).

Table 1 Kinetic parameters for the adsorption of Cr(VI) onto DCTA/E/MGO

Kinetic parameter		10 mg L^{-1}	20 mg L^{-1}	40 mg L^{-1}
Pseudo-first-order model		$q_{e,exp}$ = 66.34	$q_{e,exp}$ = 70.49	$q_{e,exp}$ = 76.71
	k_1 (min^{-1})	2.46×10^{-3}	2.40×10^{-3}	2.58×10^{-3}
	$q_{e,1}$ (mg g^{-1})	25.95	30.12	36.94
	R^2	0.894	0.911	0.955
Pseudo-second-order model	k_2 (g mg^{-1} min^{-1})	5.92×10^{-4}	4.68×10^{-4}	3.55×10^{-4}
	$q_{e,2}$ (mg g^{-1})	66.53	70.72	77.28
	R^2	0.999	0.998	0.998

To highlight the influence of diffusion on the adsorption mechanism of Cr(VI), the kinetic data were analyzed by applying the intraparticle diffusion model, which can be described as follows:[29]

$$q_t = K_d t^{0.5} + I \quad (4)$$

where q_t (mg g^{-1}) is the adsorption capacity at time t; K_d is the intraparticle diffusion rate constant (mg g^{-1} $min^{-1/2}$); I is a constant that gives idea about the thickness of the boundary layer. The larger value of I, the greater the boundary layer effect will be.[30]

If the plot q_t *versus* $t^{0.5}$ is linear and passes through the origin, the intraparticle diffusion is the only rate-limiting step; if the plot presents multilinearity, the adsorption process is controlled by two or more steps.[28] As can be seen from Fig. 4d, there are three processes controlling the adsorption rate: (i) the first sharper portions may be attributed to the film diffusion; (ii) the second linear portions are the gradual adsorption stages, where the intra-particle diffusion is rate-controlling step; and (iii) the third portions are final equilibrium stages where intra-particle diffusion starts to slow down due to low adsorbate concentration in aqueous solution as well as less number of available adsorption sites.[31] Therefore, the overall rate-limiting step involves both film diffusion and intraparticle diffusion.

3.3. Adsorption isotherm and thermodynamics

The equilibrium adsorption isotherm is studied in detail, since it could provide information about the surface properties of adsorbent and the adsorption behavior. In this work, the adsorption isotherms of Cr(VI) were investigated at 288, 303 and 318 K, respectively. Since Langmuir and Freundlich isotherm models are commonly used in description of liquid–solid systems, they were applied to simulate the experimental data of the adsorption processes.[32] The Langmuir model is based on the assumption that monolayer surface adsorption occurs on specific homogeneous sites without any interaction between the adsorbed pollutants.[33] The equation is commonly described as:[34]

$$q_e = \frac{K_L q_m C_e}{1 + K_L C_e} \quad (5)$$

where C_e is the equilibrium concentration (mg L^{-1}); q_e is the amount of metal ion adsorbed (mg g^{-1}); q_m is the theoretical saturation capacity of the monolayer (mg g^{-1}); K_L is a constant related to the affinity of the binding sites (L mg^{-1}). The Freundlich model assumes the adsorption on a heterogeneous surface without saturation of adsorbent binding sites. It can be represented by the following equation:[35]

$$q_e = K_F C_e^{1/n} \quad (6)$$

where K_F (mg g^{-1}) is a unit capacity coefficient and n is the Freundlich parameter related to the intensity of adsorption, which varies with the heterogeneity of the material. If n values are in the range $1 < n < 10$, the adsorption process is favourable, then the adsorption capacity increases and new adsorption sites occur.[36,37]

The Langmuir and Freundlich adsorption isotherms obtained using the nonlinear method are shown in Fig. 5, and the related parameters of the two models are listed in Table 2. From the correlation coefficients (R^2) and the fitting curves, the experimental data are fitted better by the Freundlich model than by the Langmuir model within the studied temperature range. The better fitting of the Freundlich isotherm indicates that the surface of the DCTA/E/MGO is likely to be heterogeneous. Moreover, all the values of Freundlich constant n (Table 2) in this study are within the beneficial adsorption range, which indicates that the DCTA/E/MGO composite can be used as an effective adsorbent.

The thermodynamic parameters provide in-depth information about internal energy changes that are associated with

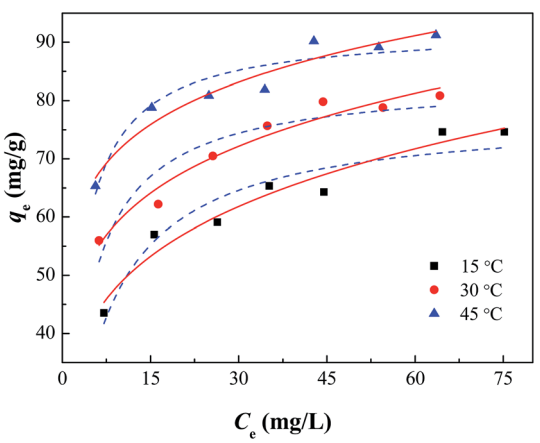

Fig. 5 Langmuir and Freundlich non-linear plots of sorption isotherms for Cr(VI) onto DCTA/E/MGO at 15, 30 and 45 °C. The solid lines are Langmuir model simulation, and the dashed lines are Freundlich model simulation (pH = 3.0 ± 0.1, t = 24 h).

Table 2 Parameters for Langmuir and Freundlich isotherm models at different temperatures

	Langmuir model			Freundlich model		
T (K)	q_{max} (mg g^{-1})	K_L (L mg^{-1})	R^2	K_F (L mg^{-1})	n	R^2
288.15	77.75	0.163	0.900	29.78	4.66	0.950
303.15	83.66	0.267	0.861	40.33	5.84	0.953
318.15	92.27	0.401	0.892	53.07	7.57	0.933

adsorption. The standard free-energy change (ΔG°), the standard enthalpy change (ΔH°), and the standard entropy change (ΔS°) are calculated from the temperature-dependent adsorption isotherms to evaluate the feasibility and exothermic nature of the adsorption process. These parameters can be calculated using the following equations:

$$\Delta G^\circ = -RT \ln K^\circ \quad (7)$$

$$\ln K^\circ = -\frac{\Delta H^\circ}{RT} + \frac{\Delta S^\circ}{R} \quad (8)$$

where R (8.314 J mol^{-1} K^{-1}) is the universal gas constant, T (K) is the absolute temperature and K° could be calculated by plotting $\ln K_d$ ($K_d = q_e/C_e$) *versus* C_e and extrapolating C_e to zero.[38] The values of ΔH° and ΔS° were calculated from the slope and intercept of a plot of $\ln K^\circ$ against $1/T$. The calculated results are given in Table 3.

The ΔG° values are negative, which indicated the spontaneity of the adsorption process. Values of ΔG° decreased slightly with the increase of temperature, which revealed the improvement of the adsorption by increasing the temperature. The positive ΔH° value suggested the endothermic nature of adsorption, which agreed well with the result that the adsorption of Cr(VI) increased along with the increase of temperature (Fig. 4). In addition, the positive ΔS° indicated that the degrees of freedom increased at the solid–liquid interface during the adsorption process.[3]

Table 3 Thermodynamic parameters of Cr(VI) adsorption on DCTA/E/MGO

Temperature (K)	$\ln K^\circ$	ΔG° (kJ mol^{-1})	ΔH° (kJ mol^{-1})	ΔS° (J K^{-1} mol^{-1})	R^2
288.15	0.511	−1.224	7.65	30.86	0.978
303.15	0.696	−1.754			
318.15	0.811	−2.145			

3.4. Effect of the solution pH

Solution pH is a significant controlling factor in adsorption process due to its effect on surface charge of the adsorbent, speciation of adsorbate and the degree of ionization.[38] The adsorption of Cr(VI) onto DCTA/E/MGO and MGO as functions of solution pH is presented in Fig. 6a. The results indicate that the adsorption of Cr(VI) shows strong dependence on solution pH. The adsorption capacities of DCTA/E/MGO and MGO for Cr(VI) are found to decrease drastically with the increase of pH ranging from 2.0 to 9.0. Other workers have reported similar phenomena for the removal of Cr(VI) by modified GO.[17,39]

In aqueous solutions, Cr(VI) exists in different ionic forms such as chromate (CrO_4^{2-}), dichromate ($Cr_2O_7^{2-}$) and hydrogen chromate ($HCrO_4^-$), depending on the solution pH and the Cr(VI) concentration.[1] In the pH range of 1.0–6.0, $HCrO_4^-$ is the predominant Cr(VI) species. As pH increases, the predominant species is CrO_4^{2-}.[3] At low pH, the large number of protons can easily coordinate with the functional groups on the material surface, which makes the material surface more positive. Thus, higher adsorption capacity at low pH can be explained by the strong electrostatic attraction between the positively charged adsorbent surface and the negatively charged chromate ions. Besides, lower adsorption capacity of Cr(VI) in high pH environment may be due to the dual competition of the anions (CrO_4^{2-} and OH^-) adsorbed on the surface of the adsorbent.[40]

The q_{max} value of Cr(VI) adsorption on DCTA/E/MGO is about 80 mg g^{-1}, which is obviously higher than that of MGO (48 mg g^{-1}) and other adsorbents, such as ethylenediamine functionalized Fe_3O_4 (61.35 mg g^{-1}),[27] magnetic cyclodextrin–chitosan/graphene oxide (67.66 mg g^{-1})[17] and cyclodextrin/ethylenediamine/magnetic graphene oxide (68.41 mg g^{-1}).[8] It can be seen that the DCTA/E/MGO has higher sorption

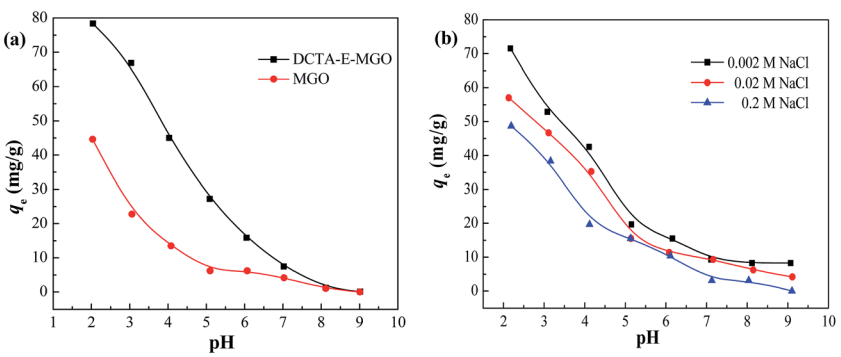

Fig. 6 (a) pH profile of Cr(VI) sorption on DCTA/E/MGO and MGO; (b) effect of ionic strength on Cr(VI) sorption ($C_{Cr(VI)\ initial}$ = 20 mg L^{-1}, T = 30 °C, t = 24 h).

capacity. DCTA and ethylenediamine have two types of reactive functional groups, carboxyl groups and amino groups, which act as chelation sites and increase the adsorption capacity.

3.5. Effect of ionic strength

The effect of ionic strength on the adsorption of Cr(VI) on DCTA/E/MGO was studied by carrying out a series of experiments at three different NaCl concentrations. As seen from Fig. 6b, the adsorption of Cr(VI) on DCTA/E/MGO decreased as the NaCl concentration ranked from 0.002 to 0.2 M. This phenomenon can be attributed to the following three reasons: (1) competition of Cl^- with Cr(VI) for the adsorption sites on DCTA/E/MGO results in the decrease of the uptake capacity.[8] (2) The increase in NaCl concentration increases the screening effect between the negatively charged Cr(VI) in solution and the positively charged adsorbent surface.[41] (3) Increased ionic strength reduces electrostatic repulsion, thereby increasing DCTA/E/MGO particle aggregation. These effects reduce the amount of available binding sites and also decrease the adsorption of Cr(VI).[42]

3.6. Proposed mechanisms of adsorption

According to the above theories and discussions, we can get that both chemisorption and physisorption are involved in the Cr(VI) adsorption process. The adsorption of Cr(VI) onto DCTA/E/MGO may be attributed to surface electrostatic attraction, coordination and hydrogen bonding. The first possible mechanism is adsorption by electrostatic forces of the protonated sites ($-OH_2^+$ and $-COOH_2^+$) on the DCTA/E/MGO surface and the negative charge of the $HCrO_4^-$, which results in complex formation.[43] The possible reactions are shown in eqn (9) and (10).

$$\equiv C\text{–}OH + H_3O^+ + HCrO_4^- \rightarrow \equiv C\text{–}OH_2^+\cdots HCrO_4^- + H_2O \quad (9)$$

$$\equiv COOH + H_3O^+ + HCrO_4^- \rightarrow \equiv COOH_2^+\cdots HCrO_4^- + H_2O \quad (10)$$

where ≡C represents the surface of DCTA/E/MGO. Besides, the DCTA grafted on the MGO surface can form complexes with Cr(VI) ions by chelation. The hydroxyl groups and nitrogen groups on the surfaces of DCTA/E/MGO have lone pairs of electrons for donation, and the Cr(VI) have vacant orbitals that can accept electron pairs from donor atoms and form coordinate covalent bonds. In addition to the above two possible mechanisms, another mechanism of adsorption of Cr(VI) on DCTA/E/MGO may involve the interaction between $HCrO_4^-$ and surface groups of DCTA/E/MGO by the formation of hydrogen bonding.[8,38]

$$\equiv C\text{–}OH + [Cr(mH_2O)]^{6+} \rightarrow \equiv C\text{–}OH\cdots[Cr(mH_2O)]^{6+} \quad (11)$$

$$\equiv COOH + [Cr(mH_2O)]^{6+} \rightarrow \equiv COOH\cdots[Cr(mH_2O)]^{6+} \quad (12)$$

4. Conclusions

The analysis results of FESEM, TEM, BET, XRD, FT-IR and XPS indicated that the DCTA/E/MGO composite was successfully prepared and it was more effective for Cr(VI) removal from water. The adsorption followed pseudo-second-order kinetic model. The equilibrium data were well-modeled by the Freundlich isotherm model. Decontamination of Cr(VI) was found to be more effective at higher temperature and lower pH range. Besides, the presence of NaCl in the solution has a negative influence on the adsorption process. Adsorption mechanisms proposed in this study included the electrostatic interaction, coordination and hydrogen bonding. In summary, the novel DCTA/E/MGO composite can be utilized as an efficient adsorbent for the Cr(VI) removal.

Acknowledgements

The authors would like to thank financial support from the National Natural Science Foundation of China (Grant no. 41271332 and 51478470) and the Hunan Provincial Innovation Foundation For Postgraduate (Grant no. CX2012B138).

References

1 W. Liu, J. Zhang, C. Zhang and L. Ren, *Chem. Eng. J.*, 2012, **189–190**, 295–302.
2 S. Luo, X. Xu, G. Zhou, C. Liu, Y. Tang and Y. Liu, *J. Hazard. Mater.*, 2014, **274**, 145–155.
3 X. J. Hu, J. S. Wang, Y. G. Liu, X. Li, G. M. Zeng, Z. L. Bao, X. X. Zeng, A. W. Chen and F. Long, *J. Hazard. Mater.*, 2011, **185**, 306–314.
4 X.-J. Hu, Y.-G. Liu, H. Wang, A.-W. Chen, G.-M. Zeng, S.-M. Liu, Y.-M. Guo, X. Hu, T.-T. Li, Y.-Q. Wang, L. Zhou and S.-H. Liu, *Sep. Purif. Technol.*, 2013, **108**, 189–195.
5 C. J. Madadrang, H. Y. Kim, G. Gao, N. Wang, J. Zhu, H. Feng, M. Gorring, M. L. Kasner and S. Hou, *ACS Appl. Mater. Interfaces*, 2012, **4**, 1186–1193.
6 S. Stankovich, D. A. Dikin, G. H. Dommett, K. M. Kohlhaas, E. J. Zimney, E. A. Stach, R. D. Piner, S. T. Nguyen and R. S. Ruoff, *Nature*, 2006, **442**, 282–286.
7 J. Li, S. Zhang, C. Chen, G. Zhao, X. Yang, J. Li and X. Wang, *ACS Appl. Mater. Interfaces*, 2012, **4**, 4991–5000.
8 H. Wang, Y. G. Liu, G. M. Zeng, X. J. Hu, X. Hu, T. T. Li, H. Y. Li, Y. Q. Wang and L. H. Jiang, *Carbohydr. Polym.*, 2014, **113**, 166–173.
9 L. Fan, C. Luo, M. Sun, X. Li and H. Qiu, *Colloids Surf., B*, 2013, **103**, 523–529.
10 H.-L. Ma, Y. Zhang, Q.-H. Hu, D. Yan, Z.-Z. Yu and M. Zhai, *J. Mater. Chem.*, 2012, **22**, 5914–5916.
11 E. A. Gautier, R. T. Gettar, R. E. Servant and D. A. Batistoni, *J. Chromatogr. A*, 1995, **706**, 115–119.
12 E. Norkus, J. Vaičiūnienė and T. Vuorinen, *Carbohydr. Polym.*, 2006, **66**, 316–320.
13 S. T. Yang, Y. Chang, H. Wang, G. Liu, S. Chen, Y. Wang, Y. Liu and A. Cao, *J. Colloid Interface Sci.*, 2010, **351**, 122–127.

14 X.-J. Hu, Y.-G. Liu, H. Wang, G.-M. Zeng, X. Hu, Y.-M. Guo, T.-T. Li, A.-W. Chen, L.-H. Jiang and F.-Y. Guo, *Chem. Eng. Res. Des.*, 2015, **93**, 675–683.
15 D. Depan, B. Girase, J. S. Shah and R. D. Misra, *Acta Biomater.*, 2011, **7**, 3432–3445.
16 C. L. Lulu Fan, M. Sun, X. Li, F. Lu and H. Qiu, *Bioresour. Technol.*, 2012, **114**, 703–706.
17 L. Li, L. Fan, M. Sun, H. Qiu, X. Li, H. Duan and C. Luo, *Colloids Surf., B*, 2013, **107**, 76–83.
18 H. Wang, X. Yuan, Y. Wu, X. Chen, L. Leng, H. Wang, H. Li and G. Zeng, *Chem. Eng. J.*, 2015, **262**, 597–606.
19 M. Zhang, Y. Wang, X. Jia, M. He, M. Xu, S. Yang and C. Zhang, *Talanta*, 2014, **120**, 376–385.
20 D. Sebben and P. Pendleton, *Spectrochim. Acta, Part A*, 2014, **132**, 706–712.
21 T. Siva, K. Kamaraj, V. Karpakam and S. Sathiyanarayanan, *Prog. Org. Coat.*, 2013, **76**, 581–588.
22 J. Liu, G. Chen and M. Jiang, *Macromolecules*, 2011, **44**, 7682–7691.
23 X. Song, Y. Yang, J. Liu and H. Zhao, *Langmuir*, 2011, **27**, 1186–1191.
24 H. Min, P. L. Girard-Lauriault, T. Gross, A. Lippitz, P. Dietrich and W. E. Unger, *Anal. Bioanal. Chem.*, 2012, **403**, 613–623.
25 J. L. Gong, B. Wang, G. M. Zeng, C. P. Yang, C. G. Niu, Q. Y. Niu, W. J. Zhou and Y. Liang, *J. Hazard. Mater.*, 2009, **164**, 1517–1522.
26 W. Plazinski, W. Rudzinski and A. Plazinska, *Adv. Colloid Interface Sci.*, 2009, **152**, 2–13.
27 Y. G. Zhao, H. Y. Shen, S. D. Pan and M. Q. Hu, *J. Hazard. Mater.*, 2010, **182**, 295–302.
28 C. Balan, I. Volf and D. Bilba, *Chem. Ind. Chem. Eng. Q.*, 2013, **19**, 615–628.
29 Z. A. ALOthman, M. Naushad and R. Ali, *Environ. Sci. Pollut. Res. Int.*, 2013, **20**, 3351–3365.
30 L. Zhang, X. Q. Jiang, T. C. Xu, L. J. Yang, Y. Y. Zhang and H. J. Jin, *Ind. Eng. Chem. Res.*, 2012, **51**, 5577–5584.
31 J. Lin, Y. Zhan and Z. Zhu, *Colloids Surf., A*, 2011, **384**, 9–16.
32 D. G. Kinniburgh, *Environ. Sci. Technol.*, 1986, **20**, 895–904.
33 L. Wang, W. Liu, T. Wang and J. Ni, *Chem. Eng. J.*, 2013, **225**, 153–163.
34 X. Mi, G. Huang, W. Xie, W. Wang, Y. Liu and J. Gao, *Carbon*, 2012, **50**, 4856–4864.
35 E. Repo, J. K. Warchol, T. A. Kurniawan and M. E. T. Sillanpää, *Chem. Eng. J.*, 2010, **161**, 73–82.
36 S. Basha and Z. V. P. Murthy, *Process Biochem.*, 2007, **42**, 1521–1529.
37 C. H. Wu, *J. Hazard. Mater.*, 2007, **144**, 93–100.
38 J. Xu, L. Wang and Y. Zhu, *Langmuir*, 2012, **28**, 8418–8425.
39 A. S. K. Kumar, S. S. Kakan and N. Rajesh, *Chem. Eng. J.*, 2013, **230**, 328–337.
40 U. K. Garg, M. P. Kaur, V. K. Garg and D. Sud, *J. Hazard. Mater.*, 2007, **140**, 60–68.
41 C. Moreno-Castilla, M. A. Ä. lvarez-Merino, M. V. López-Ramón and J. Rivera-Utrilla, *Langmuir*, 2004, **20**, 8142–8148.
42 X. J. Hu, Y. G. Liu, G. M. Zeng, S. H. You, H. Wang, X. Hu, Y. M. Guo, X. F. Tan and F. Y. Guo, *J. Colloid Interface Sci.*, 2014, **435**, 138–144.
43 A. K. Giri, R. Patel and S. Mandal, *Chem. Eng. J.*, 2012, **185–186**, 71–81.